Two-Parameter Model of Barred Galaxies and its Testification

Jin He

Wuhan FutureSpace Scientific Corporation Limited,
Wuhan, Hubei 430074, China
E-mail: mathnob@yahoo.com

Abstract Natural structure is unique and galaxies are natural structure. In our previous work, we showed that rational structure is unique. In this paper, the unique two-parameter rational structure is used to model barred galaxies. The model fits to galaxy images satisfactorily and the prediction on galaxy arms is consistent with observation. Today the accepted theory applied to galaxies is Newton's universal gravity which, however, fails to galactic observation generally. Accordingly, dark matter was introduced but has never been observed. A simple glimpse of the images of edge-on spiral galaxies suggests that Newton's concept of action at a distance should be rejected. It is hard to imagine that the stars far away from the galaxy center suffer an instant force from the center. In our previous work we suggested a new universal gravity which generalizes Newton's one and is uniquely determined by rational structure. The new gravity results from local curvature of Darwin surfaces and simply explains the constant rotation curves. In this paper, a preliminary study on the new gravity with the traditional galactic dynamic is presented which predicts the exponential disk of ordinary spiral galaxies and constant rotation curves uniquely.

keywords: Maxwellian Distribution, Spiral Galaxy, Rational Structure, Exponential Disk
PACS: 98.52.Nr, 05.20.-y

Contents

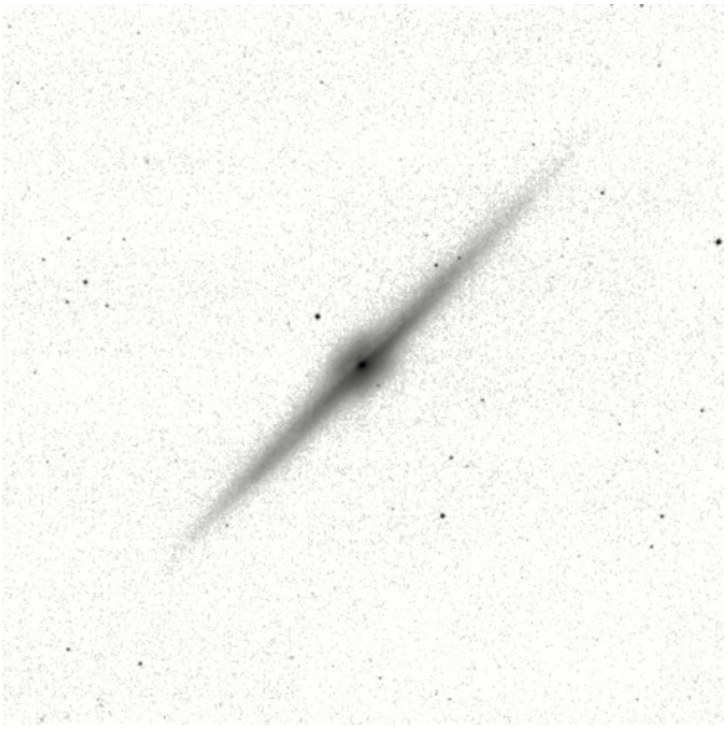

Figure 1: A longer-wavelength image of edge-on spiral galaxy NGC 4565 (Courtesy of Jarrett *et al* [1]). The central bulge is easily recognized. The disk density is the product of that in perpendicular direction and that in horizontal direction (see (50)).

1 Introduction

We humans live in a natural world whose research is called the natural science. In the natural world, there exists one kind of structure which is beyond the scope of human laboratorial experiment. It is the structure of galaxies. To humans' surprise, galaxy structure is much simpler than that on Earth. Relatively independent galaxies are either 3-dimensional (elliptical galaxies) or disk-shaped (spiral galaxies ignoring their central bulges; see Figure 1 and [1]). There are two types of spiral galaxies. A barred galaxy has additional bar structure. A spiral galaxy without bar structure is called an ordinary spiral. The main structure of ordinary spiral galaxies is an axisymmetric disk, with the stellar density decreasing exponentially along radial direction. It is the so-called exponential disk,

$$\ln \rho(x, y) = f(x, y) \sim -r \tag{1}$$

where $r = \sqrt{x^2 + y^2}$. Different from elliptical galaxies, spiral galaxies are subject to wavelike perturbation. The perturbation brings about arm structure of spiral shape. This is why they are named the spirals. However, the formation of galaxy structure has never been explained fundamentally.

We initiated an explanation with the simple concept of rational structure [2]. A distribution of stars in a plane is not arbitrary. There exists a net of orthogonal curves in the plane. If the matter density on one side of the curve is in constant ratio to the one on the other side then the curve is called a Darwin curve or a proportion curve. Such a structure of material distribution with an orthogonal net of Darwin curves is called a rational structure. The exponential disk of ordinary spiral galaxies is a rational structure. It has many nets of orthogonal Darwin curves; the curves are called golden spirals or

logarithmic spirals. Our idea also allows for some perturbation to rational structure to grow arms. The perturbation still meets the principle of constant ratios: to achieve a minimum perturbation, galaxy arms try to develop along the curves of constant ratios, that is, along the Darwin curves [3-5]. Astronomical observation does show that the arms of ordinary spiral galaxies follow Darwin curves. Now the important question is: are barred galaxies the rational structure? If so, are their arms following Darwin curves? This paper is devoted to these questions.

Currently the accepted theory applied to galaxies is Newton's universal gravity which, in actuality, is a theory of two bodies. Furthermore, it is a theory of action at a distance. To study the free motion of many stars in a galaxy, people employ a probability function called the distribution function (DF) whose integration over its whole domain, i. e., stellar position and velocity, is the total number of stars in the galaxy [6]. The law of mass conservation is used to constrain DF. Accordingly an equation called the collisionless Boltzmann equation, is derived. Integration of the equation over velocity space gives the Jeans equations which are used to study such local quantities as velocity dispersion, stability, etc. However, the law of mass conservation alone cannot predict the natural spacial distribution of many bodies. Therefore, the Boltzmann equation always involves a quantity called the gravitational potential Φ which is derived from or modeled to the observed galaxy stellar distribution based on Poisson's equation. This theory of galactic dynamics has been used to predict kinematical phenomena. These predictions do not match galaxy observation generally. The first example was presented by Zwichy [7]. Another well known example is the problem of constant rotation curves. To maintain the status of Newton's theory, people introduced the concept of dark matter which, however, has never been observed directly.

Our concept of rational structure, however, determines uniquely a new gravity which generalizes that of Newton [8]. The new gravity is resulted from local curvature of Darwin surfaces and explains the problem of constant rotation curves simply. This is because astronomical observation shows that stellar density in spiral galaxies keeps constant ratios in the vertical direction to the galaxy disks and the new gravity must be parallel to the disk if we ignore the weak contribution from galaxy bulges and halos. It is the parallel gravity that requires constant rotation curves [8]. In this paper a preliminary study on the new gravity with the traditional galactic dynamic is presented which predicts the exponential disk of ordinary spiral galaxies.

Section 2 is the introduction of the two parameter model. Section 3 is devoted to its testification in three ways: firstly fitting to longer wavelength galaxy images, secondly simulating galaxy arms, and thirdly predicting the stellar density distribution with the new gravity in the spirit of traditional galactic dynamic. The final Section is conclusion.

2 Two-Parameter Model

2.1 Rational structure theory review

We had spent about twelve years looking for the general solution to rational structure. It was achieved in our previous work [9]. The fundamental idea of rational structure is the

orthogonal net of Darwin curves

$$\begin{cases} x = x(\lambda, \mu), \\ y = y(\lambda, \mu) \end{cases} \tag{2}$$

The basic quantities describing the curves are their line magnitudes, $P(\lambda, \mu) = \sqrt{x'^2_\lambda + y'^2_\lambda}$, $Q(\lambda, \mu) = \sqrt{x'^2_\mu + y'^2_\mu}$. We proved that an orthogonal net of curves is equivalent to an analytic complex function [9]. Therefore, we can always choose x and y to be the real and imaginary parts of an analytic complex function $\varsigma(\lambda, \mu) = x(\lambda, \mu) + \mathrm{i}\, y(\lambda, \mu)$. That is, we have the Cauchy-Riemann equations

$$\begin{cases} x'_\lambda = y'_\mu, \\ x'_\mu = -y'_\lambda \end{cases} \tag{3}$$

Accordingly, the two line magnitudes become equivalent

$$P = \sqrt{x'^2_\lambda + x'^2_\mu} = \sqrt{y'^2_\lambda + y'^2_\mu} = Q \tag{4}$$

The fundamental quantities describing the rational structure are the directional derivatives to the logarithmic density ($f = \ln \rho$) along the orthogonal net of curves, $\hat{u}(\lambda, \mu), \hat{v}(\lambda, \mu)$. The parallel law is that they are the functions of single variables only, $\hat{u} = \hat{u}(\lambda),\ \hat{v} = \hat{v}(\mu)$. The skew law is that both the logarithmic density and the line magnitude are the functions of the single variable

$$\hat{C} = \hat{U}(\lambda) + \hat{V}(\mu) \tag{5}$$

where $\hat{u} = d\hat{U}(\lambda)/d\lambda, \hat{v} = d\hat{V}(\mu)/d\mu$. That is,

$$f(\hat{C}) = h \int P(C) dC \tag{6}$$

where we have introduced a common constant h so that $\hat{C} = hC$, $\hat{U} = hU$, etc. Note that natural density distribution usually requires $h < 0$. The mathematical relations among partial derivatives, directional derivatives and line magnitude are

$$\begin{aligned} f'_\lambda &= \hat{u} P(\lambda, \mu), \\ f'_\mu &= \hat{v} P(\lambda, \mu) \end{aligned} \tag{7}$$

Now we see that the formula (6) does lead to the above relations. The above formulas (6) and (7) are very important. If the line magnitude $P(C)$ does determine an orthogonal net of curves which satisfies the Cauchy-Riemann equations (3), then the resulting structure (6) must be rational. This is because the directional derivatives $\hat{u}$ and $\hat{v}$ given by the formulas (7) are single-variable functions themselves.

The paper [9] showed that the line magnitudes given by the Riccati equation with constant coefficients do determine orthogonal nets of curves which satisfy the Cauchy-Riemann equations. In fact, the Riccati equation is the necessary and sufficient condition for rational structure. Therefore, there are only a few solutions to rational structure. The solutions are denoted by Riccati-aw, Riccati-$Pw^{\frac{2n+1}{2}}$ ($n = 0, 1, 2, 3, \dots$), Riccati-Tw, and Riccati-Hw, respectively. Coincidentally, astronomical observation shows that,

ignoring those strongly interacted ones, there exist only a few types of galaxies. We know that the spacial density distribution of elliptical galaxies meets Sércic law excellently [10, 11]. The law is a power law at large radii from the center of elliptical galaxies. The spacial density distribution of spiral galaxies satisfies exponential law at those areas. A preliminary study showed that Riccati-Tw and Riccati-Hw follow the power law. This suggests that they may fit to elliptical galaxies. However, the study on elliptical galaxies is left for the future work. The current paper is focused on barred galaxies. Coincidentally, Riccati-00 is the exponential disk of ordinary spiral galaxies (see the formula (1)). Riccati-$Pw\frac{1}{2}$ is the Heaven-Breasts structure which can not be used alone to model the global structure of barred galaxies. The current paper is focused on the study of Riccati-$Pw\frac{2n+1}{2}$, $n = 1, 2, 3, \ldots$ each of which has only two parameters and is used to model the global structure of barred galaxies. In Section 2.2, we study the limiting structure ($r \to \infty$) and prove that Riccati-$Pw\frac{2n+1}{2}$ follows the new exponential law, $\log \rho(x, y) \sim -r^{(2n+3)/(2n+1)}$. In Section 3 we show that Riccati-$Pw\frac{3}{2}$ fits to barred galaxies satisfactorily. This suggests that barred galaxies may not follow the precise exponential law (1).

2.2 Limiting structure of Riccati-$Pw\frac{2n+1}{2}$

Now we study the bar model Riccati-$Pw\frac{2n+1}{2}$. That is,

$$P(C) = mC^{(2n+1)/2} \tag{8}$$

where m is a constant and $n = 1, 2, 3, \ldots$. The orthogonal curves (2) are determined by the Cauchy-Riemann equations (3) and the line magnitude

$$mC^{(2n+1)/2} = \sqrt{x_\lambda'^2 + x_\mu'^2} \tag{9}$$

The above equation leads to (see [9])

$$x_\mu' + \mathrm{i}\, x_\lambda' = m\sqrt{2A}^{2n+1} \cosh^{2n+1} \zeta \tag{10}$$

where ζ is a complex variable,

$$\zeta = \xi + \mathrm{i}\, \eta = \frac{w\lambda + \epsilon}{2} + \mathrm{i}\, \frac{w\mu + \delta}{2} \tag{11}$$

and $m, A, w, \epsilon, \delta$ are other constants. If we define

$$\nu = \sinh \zeta \tag{12}$$

and take $n = 1$ then the integration of the differential equation (10) is

$$\nu^3 + 3\nu + q = 0 \tag{13}$$

where

$$q = \tilde{y} - \mathrm{i}\, \tilde{x} = y/H - \mathrm{i}\, x/H \tag{14}$$

and $H = \frac{2m\sqrt{2A}^3}{3w}$ is a constant. This is a cubic algebraic equation. The complex number q is defined in the (x, y) plane. The solutions to the cubic equation are dependent on q only

and, accordingly, are the functions defined in the plane. Skew quantity C and rational structure f, which are dependent on the solutions only (see the following formulas (15)), are defined in the plane also. Similarly, rational structure Riccati-$Pw\frac{2n+1}{2}$ is determined by an algebraic equation of degree $2n+1$, whose skew quantity C is (see [9])

$$\begin{aligned} C &= A(\cosh(2\xi)+\cos(2\eta)) = 2A|\cosh^2\zeta| = 2A\left|1+\sinh^2\zeta\right| \\ &= 2A\left|1+\nu^2\right| \end{aligned} \tag{15}$$

and whose logarithmic density distribution is

$$f(x,y) = h\int P(C)dC = hm\int C^{(2n+1)/2}dC = \frac{2hm}{2n+3}C^{(2n+3)/2} \tag{16}$$

Denoting ν by

$$\nu = \nu_a + \mathrm{i}\,\nu_b \tag{17}$$

we have

$$C = 2A\left|1+\nu^2\right| = 2A\sqrt{4\nu_a^2+(1-\nu_a^2-\nu_b^2)^2} \tag{18}$$

So far, the formulas presented are exact mathematical solutions. Now we study the limiting structure, that is, the structure far away from the center: $r\to\infty$. The algebraic equation of degree $2n+1$ gives

$$|\nu| \sim |q|^{1/(2n+1)} \sim r^{1/(2n+1)} \tag{19}$$

Therefore,

$$C \sim |\nu|^2 \sim r^{2/(2n+1)} \tag{20}$$

and

$$\ln\rho(x,y) \sim f(x,y) \sim -r^{(2n+3)/(2n+1)}, \quad r\to\infty \tag{21}$$

It approaches the precise exponential law if $n\to\infty$. We know that $n=0$ corresponds to the famous Heaven Breasts structure. A preliminary study on Riccati-$Pw\frac{3}{2}$ is presented in [9]. It generates three rational structures, and two of them display the pattern similar to Heaven-Breasts. However, the third solution does display a bar pattern. All three solutions display the same limiting structure

$$\ln\rho(x,y) \sim -r^{5/3}, \quad r\to\infty \tag{22}$$

A preliminary study showed that Riccati-$Pw\frac{5}{2}$ displays at least five rational structures. Three of them are similar to Heaven Breasts. Of the other two, one displays a web-shaped pattern and the other displays a bar pattern. The bar pattern is similar to that of Riccati-$Pw\frac{3}{2}$. Therefore, we would expect Riccati-$Pw\frac{2n+1}{2}$, $n=1,2,3,\ldots$, to share similar characteristics. Accordingly, this paper is devoted to the study of Riccati-$Pw\frac{3}{2}$ only, and Section 2.3 presents the global formulas of its bar pattern.

2.3 Formulas of Riccati-$Pw\frac{3}{2}$

Barred galaxies are generally bi-laterally symmetric. The cubic algebraic equation does have bi-laterally symmetric solution. The proof is as follows. If ν is a solution to (13) then its conjugate $\bar{\nu}$ must be a solution to the following equation,

$$\nu^3 + 3\nu + \bar{q} = 0 \tag{23}$$

Because $|1+\nu^2| \equiv |1+\bar{\nu}^2|$ (see formula (18)), the resulting rational structure is symmetric about the x-axis. Assuming any number $z = a + \mathrm{i}\ b$, we define

$$\ddot{z} = -a + \mathrm{i}\ b \tag{24}$$

It is straightforward to show that

$$\ddot{z^n} = (\ddot{z})^n\,, \quad n = 1, 3, 5, 7, \ldots \tag{25}$$

Therefore, if ν is a solution to (13), $\ddot{\nu}$ must be a solution to the following equation,

$$\nu^3 + 3\nu + \ddot{q} = 0. \tag{26}$$

Because $|1+\nu^2| \equiv |1+\ddot{\nu}^2|$ (see formula (18)), the resulting rational structure is symmetric about the y-axis too. Finally, we have proved that our rational structure is bi-laterally symmetric about both x-axis and y-axis. Accordingly, we will always derive the formulas of rational structure in a quadrant of the (x, y) plane. From now on, our rational structure is defined only in the second quadrant

$$\tilde{x} < 0, \quad \tilde{y} > 0 \tag{27}$$

Therefore, $q = \tilde{y} - \mathrm{i}\ \tilde{x}$ is always positioned in the first quadrant.

We use Cadano's method to solve the cubic equation as we did in [9]. We will use the same symbols in [9]. The solutions to (13) are based on a quadratic equation

$$\kappa^2 + q\kappa - 1 = 0 \tag{28}$$

whose coefficient of the linear term is the variable q and the constant term is -1. The constant term would be ignored if we study the limiting structure. Therefore, we introduce a symbol χ to always denote the constant term,

$$\kappa^2 + q\kappa - \chi/2 = 0 \tag{29}$$

where

$$\chi = 2 \tag{30}$$

Now we solve the quadratic equation. Its discriminant is

$$\Delta = q^2 + \chi^2 \tag{31}$$

We introduce the symbols φ and θ,

$$\begin{array}{l} q = \tilde{y} - \mathrm{i}\ \tilde{x} = \tilde{r}(\cos\varphi + \mathrm{i}\ \sin\varphi), \\ \Delta = \sqrt{(\chi^2 - \tilde{r}^2)^2 + 4\chi^2\tilde{y}^2}(\cos\theta + \mathrm{i}\ \sin\theta) \end{array} \tag{32}$$

where $\tilde{r} = \sqrt{\tilde{x}^2 + \tilde{y}^2}$ and

$$0 \le \varphi \le \frac{\pi}{2} \tag{33}$$

Now we have the two roots κ_1, κ_2

$$\begin{aligned} \kappa_1 &= \phi_1 + \mathrm{i}\ \phi_2 = \tfrac{1}{2}\left(-\tilde{y} + \sqrt{|\Delta|}\cos(\theta/2) + \mathrm{i}\ (\tilde{x} + \sqrt{|\Delta|}\sin(\theta/2))\right), \\ \kappa_2 &= \psi_1 + \mathrm{i}\ \psi_2 = \tfrac{1}{2}\left(-\tilde{y} - \sqrt{|\Delta|}\cos(\theta/2) + \mathrm{i}\ (\tilde{x} - \sqrt{|\Delta|}\sin(\theta/2))\right) \end{aligned} \tag{34}$$

Firstly, we calculate the moduli and phases of the two roots. Let arg1 and arg2 be their phases, respectively. For this paper, we always take

$$\begin{aligned} \mathrm{arg1} &= [\phi_2]\arccos\tfrac{\phi_1}{|\kappa_1|}, \\ \mathrm{arg2} &= [\psi_2]\arccos\tfrac{\psi_1}{|\kappa_2|} \end{aligned} \tag{35}$$

where $[\phi_2]$ and $[\psi_2]$ are the signs of the numbers ϕ_2 and ψ_2, respectively. It is straightforward to show that

$$\begin{aligned} |\kappa_1|^2 &= \tfrac{\tilde{r}^2+|\Delta|}{4} + \tfrac{\sqrt{|\Delta|}}{2}\left(\tilde{x}\sin\tfrac{\theta}{2} - \tilde{y}\cos\tfrac{\theta}{2}\right), \\ |\kappa_2|^2 &= \tfrac{\tilde{r}^2+|\Delta|}{4} - \tfrac{\sqrt{|\Delta|}}{2}\left(\tilde{x}\sin\tfrac{\theta}{2} - \tilde{y}\cos\tfrac{\theta}{2}\right) \end{aligned} \tag{36}$$

According to Cadano's method, each solution to the original cubic equation must be the sum of one of the cubic roots to κ_1 and one of the cubic roots to κ_2. Finally, the solution ν which corresponds to the required bar pattern is $\nu = \beta_1 + \gamma_1$ where

$$\begin{aligned} \beta_1 &= |\kappa_1|^{1/3} e^{\mathrm{i}(\mathrm{arg1}+2\pi)/3}, \\ \gamma_1 &= |\kappa_2|^{1/3} e^{\mathrm{i}(\mathrm{arg2}+2\pi)/3} \end{aligned} \tag{37}$$

Note that the above formulas may be wrong if the quadrant condition (27) is not satisfied.

The above are the formulas of the model of Riccati-$Pw\frac{3}{2}$ which are required for the display of rational bar. The bar model has only two parameters. Given a galaxy image, we do not know the physical size of the real galaxy. Our focus is on the galaxy patterns. The image (usually square) is without coordinates. The model, whose variables $\tilde{x}$ and $\tilde{y}$ are fitted to the image pattern, establishes coordinates for the image. The first parameter is the side length L of the image. That is,

$$|\tilde{x}| \le L/2, \quad |\tilde{y}| \le L/2 \tag{38}$$

A larger L corresponds to a rounder bar pattern. The second parameter is the factor

$$K = \frac{2hm}{5}(2A)^{5/2} \tag{39}$$

which is shown in (16). The parameter describes the fatness of the bar. Smaller $|K|$ corresponds to a fatter bar. The third parameter ρ_0 where $\rho(x, y) = \rho_0 \exp(f(x, y))$, is the common factor to the whole stellar light distribution, which, however, is not relevant to galaxy pattern.

Table 1: Barred galaxy image simulation

galaxy NGC	sky level	ρ_0	image length $''$	fitting length L	fatness K
3275	1010	740	110	13.2	-0.15
4930	1000	720	108.3	6.4	-0.28
5701	990	1360	105	8.4	-0.17
6782	1005	1100	117	9.2	-0.28

3 Testification

3.1 Fitting to barred galaxy images

In our model, galaxies are considered to be patterns of density distribution. Because a pattern is a distribution of differences and differences are equivalent to mathematical derivatives, all of our results are dependent only on the derivatives to the logarithmic stellar distribution, not on the absolute value of the distribution. That is why we are not worried about the distances of galaxies from the Earth, nor are we worried about the stellar mass to light ratios. Our model is justifiable because astronomical observation shows that relatively independent galaxies, large or small, far or near, demonstrate similar patterns. Therefore, what we want is an array of numbers (a digital image) which is proportional to the galaxy light distribution. Galaxies are considered to be natural structures, and natural structures are more complicated than their mathematical models. Accordingly, different wavelengths of galaxy images may display varied patterns. Fortunately, longer wavelength galaxy images are good approximation to the pattern of galaxy mass distribution. That is why we choose H-band images in Figures 2, 3, 4, 5, and 6. Our model of galaxy mass distribution is always based on longer wavelength galaxy images.

Before studying galaxy arms, we simulate the stellar density distribution of the galaxy so that we have an analytic formula of the distribution that is ready for the calculation of its derivatives. Table 1 is the result of the simulation for galaxies NGC 3275, 4930, 5701 and 6782. The letters L, K in the Table are the two parameters of our model which represent the fitting length (roundness) and the fatness of the simulated structure, respectively. The fitting is much better than that in [5]. This suggests that the limiting structure of barred galaxies may not follow the precise exponential law (1). Instead it may follow the new exponential law (21). The meaning of other parameters in Table 1 was explained in [5].

As displayed in Figures 2 – 6, there are apparent central lines in the simulated bar patterns which indicate that the directional derivatives to the logarithmic density across the central line are not continuous. We study it in details. We take the first order approximation. That is, we take $\chi = 0$. It is straightforward to show that the root κ_1 in (34) is zero and the root κ_2 is

$$\kappa_2 \approx -q = -\tilde{y} + \mathrm{i}\ \tilde{x} = -\tilde{r}(\cos\varphi + \mathrm{i}\ \sin\varphi) \tag{40}$$

where $0 \leq \varphi \leq \frac{\pi}{2}$ (see (32) and (33)). Therefore,

$$\begin{aligned} \nu &\approx \kappa_2^{1/3} = \tilde{r}^{1/3}\left(\cos\left(\tfrac{-\pi/2-\varphi}{3}+\tfrac{2\pi}{3}\right)+\mathrm{i}\ \sin\left(\tfrac{-\pi/2-\varphi}{3}+\tfrac{2\pi}{3}\right)\right) \\ &= \tilde{r}^{1/3}(\sin\tfrac{\varphi}{3}+\mathrm{i}\ \cos\tfrac{\varphi}{3}) \end{aligned} \tag{41}$$

This is true because our cubic equation reduces to (see (13))

$$\nu^3 \approx -q \tag{42}$$

Substituting ν into C in (18), we have in the first order approximation

$$C^2 \approx 4A^2\left(r^{4/3}+1-2r^{2/3}\cos\frac{2\varphi}{3}\right) \tag{43}$$

Along the negative x-axis, we have $\varphi = \pi/2$ and $\cos(2\varphi/3) = \cos(\pi/3)$, which indicates that the directional derivatives to the logarithmic density in the first order approximation across the x-axis are not continuous. At large radii, the discontinuity disappears.

However, we usually do not see apparent central lines in real galaxy images. There are possible explanations. Firstly, the lines are so weak and galaxies are so far away from us that the possible existence of real lines are buried in the noise of galaxy images. Secondly, galaxies are coarse distribution of discrete stars. We can determine the density of discrete stars only by counting them in volumes large enough to contain many stars. The width of the central lines is too small to be resolved in the coarse-grained galaxy images. Thirdly, the central lines in the bar patterns of Riccati-$Pw\frac{2n+1}{2}$ when $n \to \infty$, may be less apparent. These require further investigation.

3.2 Fitting to barred galaxy arms

In the traditional study of galaxy arms, people consider spiral arms to be density waves that propagate through the disk of stars and gas and form as dynamic response of the disk to some perturbations [13-16]. The wave of perturbation must take the form

$$\Phi_1(r,\phi) \sim \cos(g(r,\phi)) \tag{44}$$

where (r,ϕ) are the polar coordinates in the galaxy disk plane, and $g(r,\phi)$ is an unknown function. To achieve logarithmic arms, people have to choose

$$\Phi_1(r,\phi) \sim \cos(k\ln r + m\phi) \tag{45}$$

However, why the nature chooses such a perturbation is not explained by the traditional theory of density waves. People also proposed the theory of kinematic density waves which is solely based on the theory of Newtonian orbits of a star in some gravitational potentials. The orbits appear to be ellipses. Aligned ellipses are used to explain bar formation, and non-aligned ellipses are used to explain spiral formation. However, it is still a problem why the nature delicately arranges the ellipses to form a pair of logarithmic spirals. Furthermore, the long-term stellar orbits are not observable in the same way the electrons' orbits in an atom can not be observed.

It is straightforward to show that the consideration of bars as arms is basically wrong. Spiral arms are always accompanied by dust and gases among stars of recent birth. Therefore, in longer-wavelength images of spiral galaxies, the rich patterns of spiral arms are greatly reduced or barely seen. However, bars that are generally composed of older stars, never reduce or disappear in any wavelength of images. The dust and gases inside bars are much less than that in spiral arms. The most important difference between bars and arms is that arms are always linear-shaped while bars are always bi-laterally symmetric fat distribution of stars. Therefore, bars should be considered to be the integral parts of the whole stellar distributions.

In this paper, bars and disks are united as a unique structure, i. e., rational structure. Our idea also allows for some perturbation to rational structure to grow arms. The perturbation still meets the principle of constant ratios: to achieve a minimum perturbation, galaxy arms try to develop along the Darwin curves [3-5].

Armed with the simulated global stellar distribution, we can calculate the directional derivatives to its logarithmic distribution. The formulas of relevant derivatives can be found in the Appendix. To find Darwin curves, we are beforehand given a constant value of the derivative. We have a given point in the disk plane, and we calculate the gradient at the point. If the modulus of the gradient is greater than the given derivative then there exist two curves crossing at the point (i. e., two directions) whose perpendicular directional derivatives at the point are the given one. Note that the two curves are generally two spirals in clockwise and counter-clockwise directions, respectively. Therefore, we can use the integration methods of ordinary differential equations to solve our question, i. e., to find the Darwin curves crossing at the given point. The curves at the left panel of Figure 7 are the examples of Darwin curves. The result shows some evidence that the arms of galaxy NGC 3275 follow Darwin curves. However, there are apparent deviation from the actual arms. Here is some possible explanation. Galaxy arms may be likened to the branches in a tree. A bigger branch is composed of smaller branches. What Figure 7 shows is that the smaller branches follow Darwin curves but the bigger ones may not.

The Figure also shows the discontinuity of the directional derivatives across the central line of the bar. Some barred galaxies do demonstrate broken arms at the ends of the bars (for example, see the arms of NGC 613, 1097, 1300, 1365, 1672, 5236, 6217, 7479). Study on barred galaxy images indicates that the arms which cross the central line at roughly a right angle are usually not broken. This is consistent with our model because the perpendicular direction to the arms is roughly in the direction of the central line along which the directional derivative is smooth when crossing the line. However, any arm crossing the center line could be smooth if the value of the constant ratio was changed correspondingly when crossing the line.

3.3 Darwin surfaces and constant rotation curves

By now we have achieved the simulation of global galaxy structure and linear spiral arms. It is important to verify that the two-parameter model is really rational structure and the formulas involved have no mistakes. In fact, we proved in Section 2.1 that the skew law (6) and the mathematical identities (7) do lead to rational structure provided that the curves (2) satisfy the Cauchy-Riemann equations. In our case, the curves are the

solutions to the differential equation which involves analytic complex functions only (see (10)). Therefore, the curves must satisfy the Cauchy-Riemann equations. However, we can double check as follows. Firstly, we can prove that the rational structure equation (see [3, 9]) is satisfied. The directional derivatives along the net of curves (2) are

$$\begin{array}{l} u(\lambda) = Aw\sinh(2\xi), \\ v(\mu) = -Aw\sin(2\eta) \end{array} \tag{46}$$

The corresponding line magnitude is (8). It is simple to verify that the rational structure equation holds,

$$u(\lambda)P'_{\mu} = v(\mu)P'_{\lambda} \tag{47}$$

Secondly, we can draw the curves (2) and verify that they are orthogonal. It is hard to obtain the analytic formulas of the curves. However, they must be composed of the level curves of the two functions $u(\lambda)$ and $v(\mu)$, respectively. It is straightforward to prove the following two mathematical identities

$$\begin{array}{l} A(\cosh(2\xi) + \cos(2\eta)) = C = 2A\left|1+\nu^2\right|, \\ A(\cosh(2\xi) - \cos(2\eta)) = 2A\left|\nu\right|^2, \end{array} \tag{48}$$

Therefore,

$$\begin{array}{l} \cosh(2\xi) = \left|1+\nu^2\right| + \left|\nu\right|^2, \\ \cos(2\eta) = \left|1+\nu^2\right| - \left|\nu\right|^2 \end{array} \tag{49}$$

The level curves of the above two functions are identical to the ones of $u(\lambda)$ and $v(\mu)$, respectively. The level curves of $v(\mu)$ are demonstrated as white dashed curves at the right panel of Figure 7. The level curves of $u(\lambda)$ are supposed to be orthogonal to the white curves. The orthogonality can be verified mathematically. Here, however, we calculate the gradients of the two functions in (49) based on the formulas in the Appendix, and demonstrate their scalar product numerically with a computer program. The numerical result is that the absolute values of the product are less than 10^{-15} with an ordinary personal computer. We changed some part of the formulas on purpose, and we had the resulting values to be $\sim 10^4$. Therefore, the formulas for the barred pattern of Riccati-$Pw\frac{3}{2}$ are correct and the corresponding curves are orthogonal indeed.

The orthogonal curves look like "ellipses" and "hyperbolas". The "ellipses" do show the discontinuity of the directional derivatives across the central line of the bar (see the right panel of Figure 7). We know that Riccati-$Pw\frac{1}{2}$ is the Heaven-Breasts structure whose orthogonal curves are all co-foci ellipses and hyperbolas. Here, however, "ellipses" and "hyperbolas" have no co-foci.

Although spiral galaxies are flat and considered to be two-dimensional, they still have a certain thickness. We use z to describe the vertical direction to the disk and r to describe the horizontal direction as seen on an edge-on spiral galaxy image (see Figure 1). Astronomical observation shows that the stellar density distribution on an edge-on spiral galaxy image can be described by a formula whose variables z and r can be separated [17],

$$\rho(r,z) = \sigma(r)\,\tau(z) \tag{50}$$

This means that the ratio of galaxy light from two sides of each vertical straight line is constant along the line. That is, spiral galaxies considered to be 3-dimensional are still

rational structure. Let us use ordinary spiral galaxies as an example. The stellar density distribution of an ordinary spiral galaxy is axi-symmetric with respect to the galaxy center, and its stellar density decreases exponentially in the radial direction. Any orthogonal net of Darwin curves of an exponential disk is composed of golden spirals. However, there is a trivial net of Darwin curves which is composed of all concentric circles centered at the galaxy center and all radial lines. Therefore, if an ordinary spiral galaxy is considered to be a 3-dimensional structure, these concentric Darwin circles become coaxial Darwin cylinders and the radial lines become coaxial radial planes. That is, the orthogonal net of Darwin surfaces of ordinary spiral galaxies is composed of all coaxial cylinders and coaxial planes which are perpendicular to the galaxy disk, and all planes which are parallel to the galaxy disk. New gravity is closely related to the Darwin surfaces [8].

New Universal Gravity: To any point on a rational structure, there correspond three Darwin surfaces which pass the point and are orthogonal to each other. To any Darwin surface there exists the corresponding component of the gravitational force at the point whose direction is normal to the surface (pointing to the larger matter density) and whose magnitude is proportional to the Gaussian curvature of the surface at the point and proportional to the total mass included by the surface.

It is easy to prove that the new universal gravity is the generalization to Newton's one. This is because the Darwin surfaces of a central mass point must lead to a central force. Now we study the gravitational force field of ordinary spiral galaxies with traditional galactic dynamics. Our new gravity is still a central force because ordinary spiral galaxies are axi-symmetric. However, there is the important difference between Newton's gravity and the new one: our central force is 2-dimensional, not 3-dimensional.

The distribution function DF has two sets of arguments in the phase space, one being position and the other being velocity. If determined, DF would connect stellar density distribution to stellar kinematics. However, generally the traditional galactic dynamics with Newton's gravity failed to find a DF which matches stellar density distribution and stellar kinematics simultaneously [6]. That is the sole reason why dark matter is needed. Armed with our new gravity, however, we prove that exponential disk is the sole condition for constant rotation curves provided that Maxwellian distribution of ideal gas holds to stellar system.

A simple extension of the strong Jeans theorem to spherical system [18] permits us to conclude that the DF of a steady-state system can be expressed as a function $DF(E, L)$ where E is energy and L is the modulus of angular momentum. The simplest spherical models are those with DFs that depend on E only (see [6], pp. 222). We use relative potential Ψ and relative energy $\mathcal{E}$ (see the same reference)

$$\Psi \equiv -\Phi + \Phi_0 \text{ and } \mathcal{E} = -E + \Phi_0 = \Psi - \frac{1}{2}v^2 \tag{51}$$

where Φ_0 is a constant. Maxwellian distribution holds to classical ideal gas,

$$F(v) = Ne^{-\frac{1}{2}v^2/\sigma^2} \tag{52}$$

where N and σ are constants. Kinetic theory [19] tells us that the above is also the equilibrium Maxwell-Boltzmann distribution which would obtain if the stars were allowed

to bounce elastically off each other like molecules of a gas. Therefore, the required DF is (see [6], pp. 226)

$$DF(\mathcal{E}) = \frac{\rho_1}{(2\pi\sigma^2)^{3/2}} e^{\mathcal{E}/\sigma^2} = \frac{\rho_1}{(2\pi\sigma^2)^{3/2}} \exp^{\frac{\Psi - \frac{1}{2}v^2}{\sigma^2}} \tag{53}$$

In our case, however, the above DF must be changed into a 2-dimensional form

$$DF(\mathcal{E}) = \frac{\rho_1}{2\pi\sigma^2} e^{\mathcal{E}/\sigma^2} = \frac{\rho_1}{2\pi\sigma^2} \exp^{\frac{\Psi - \frac{1}{2}v^2}{\sigma^2}} \tag{54}$$

where

$$\mathbf{v} = (v_x, v_y) \tag{55}$$

is the 2-dimensional velocity vector in the galaxy disk plane. We decompose the velocity vector as the sum of the local standard of rest (that is, the local circular velocity $\mathbf{v}_c$) and the "microscopic" thermal motion $\mathbf{v}_{\rm th}$,

$$\mathbf{v} = \mathbf{v}_c + \mathbf{v}_{\rm th} \tag{56}$$

Therefore, $v^2 = v_x^2 + v_y^2 = (v_{cx} + v_{{\rm th}x})^2 + (v_{cy} + v_{{\rm th}y})^2$. Integrating over all thermal velocities, we have

$$\rho = \frac{\rho_1}{\sigma^2} \exp^{\frac{\Psi}{\sigma^2}} \int_0^\infty \exp^{-\frac{v^2}{2\sigma^2}} v dv = \rho_1 \exp^{\frac{\Psi}{\sigma^2}} \tag{57}$$

The 2-dimensional Poisson's equation reads

$$\frac{1}{r}\frac{d}{dr}\left(r\frac{d\Psi}{dr}\right) = -2\pi G\rho \tag{58}$$

With equation (57), we have

$$\frac{d}{dr}\left(r\frac{d\ln\rho}{dr}\right) = -\frac{2\pi G}{\sigma^2} r\rho \tag{59}$$

Integrating the above equation leads to

$$r\frac{d\ln\rho}{dr} = -\frac{G}{\sigma^2} M(r) \tag{60}$$

where $M(r)$ is the total disk mass interior to r. Note that the circular speed at r, v_c, is given by

$$v_c^2 = \frac{GM(r)}{r} \tag{61}$$

Finally, (60) leads to

$$\frac{d\ln\rho}{dr} = -\frac{v_c^2}{\sigma^2} \tag{62}$$

Now we see that the necessary and sufficient condition for the exponential disk (1) of ordinary spiral galaxies is the constant rotation curve, v_c = constant.

The above 2-dimensional Poisson's equation holds because we have a 2-dimensional central force. This is not true for barred spiral galaxies where gravity can not reduce to a central force. The new gravitational field needs further investigation, which is left for the future work. If a similar result between the stellar density distribution and the constant rotation curves for barred galaxies is proved, then the new gravity approaches to cosmic truth.

4 Conclusion

The formulas of a two-parameter rational structure model are presented and fitted to the images of four barred galaxies. The fitting is satisfactory which indicates that barred galaxies may follow a new exponential law (21). Because the exponential disk of ordinary spiral galaxies has only one parameter, the Riccati-$Pw\frac{2n+1}{2}$ bar model is promising in that it has the minimum two parameters and fits to barred galaxy images. The model also fits to barred galaxy arms without apparent contradiction and presents simple explanation to some characteristic features of arm pattern. Finally, the traditional galactic dynamics with the new gravity is applied to ordinary spiral galaxies. Assuming the well-known Maxwellian distribution of ideal gas, we proved that the exponential disk of ordinary spiral galaxies is the necessary and sufficient condition for constant rotation curves. Our model is simple and straightforward, and many astronomical and astrophysical applications are expected. If further justified, the model should point to some fundamental truth involving spiral galaxy formation.

5 Acknowledgement

The author wishes to thank Bo He for important suggestion.

References

[1] Jarrett T., Chester T., Cutri R., Schneider S. and Huchra J. (2003) Astron. J. **125**, 525

[2] He J. (2003) Astrophys. Space Sci. 283, 301

[3] He J. (2005) Ph.D. thesis, The University of Alabama (Tuscaloosa, USA)

[4] He J. (2010) Elec. J. Theo. Phys. 7, 361
He J. (2012) Submitted to Journal of Experimental and Theoretical Physics; Title "Harmonic Galaxy Structure"
viXra:1211.0020

[5] He J. (2014) Centr. Euro. J. Phys. (in press)

[6] Binney J., Tremaine S. (1987) Galactic Dynamics, 1st edition (Princeton University Press, Princeton, USA)

[7] Zwicky F. (1933) Helvetica Physica Acta 6, 110

[8] He J. (2013) Submitted to Journal of Experimental and Theoretical Physics; Title "New Universal Gravity and Rational Galaxy Structure"
viXra:1303.0114

[9] He J. (2014) Submitted to Journal of Experimental and Theoretical Physics; Title "Are Galaxies Structured by Riccati Equation? The First Graph of Rational Bar" viXra:1402.0081

[10] Sércic J. (1968) Atlas de Galaxias Australes. Observatorio Astronómico, Córdoba

[11] He J. (2008) Astrophys. Space Sci. 313, 373

[12] P. Eskridge, *et al.* Astron. J. Suppl. 143, 73 (2002)

[13] Julian W., Toomre A. (1966) ApJ 146, 810

[14] Goldreich P., Lynden-Bell D. (1965) MNRAS 130, 125

[15] Lin C. C., Shu F. (1964) ApJ 140, 646

[16] D'Onghia E., Vogelsberger M., Hernquist L. (2013) ApJ 766, 34

[17] de Grijs R., van der Kruit P. C. (1996) Astron. Astrophys. Supple. 117, 19

[18] Lynden-Bell D. (1962) MNRAS 124, 1

[19] Jeans J. H. (1940) Kinetic Theory of Gases, 1st edition (Cambridge University Press, Cambridge, Eng)

6 Appendix

$$
\begin{aligned}
\nu'_{ax} = {} & \tfrac{1}{3}|\kappa_1|^{-5/3}\left((\phi_1\phi'_{1x}+\phi_2\phi'_{2x})\cos\tfrac{\arg1+2\pi}{3}+(\phi_2\phi'_{1x}-\phi_1\phi'_{2x})\sin\tfrac{\arg1+2\pi}{3}\right)\\
& +\tfrac{1}{3}|\kappa_2|^{-5/3}\left((\psi_1\psi'_{1x}+\psi_2\psi'_{2x})\cos\tfrac{\arg2+2\pi}{3}+(\psi_2\psi'_{1x}-\psi_1\psi'_{2x})\sin\tfrac{\arg2+2\pi}{3}\right),\\
\nu'_{bx} = {} & \tfrac{1}{3}|\kappa_1|^{-5/3}\left((\phi_1\phi'_{1x}+\phi_2\phi'_{2x})\sin\tfrac{\arg1+2\pi}{3}-(\phi_2\phi'_{1x}-\phi_1\phi'_{2x})\cos\tfrac{\arg1+2\pi}{3}\right)\\
& +\tfrac{1}{3}|\kappa_2|^{-5/3}\left((\psi_1\psi'_{1x}+\psi_2\psi'_{2x})\sin\tfrac{\arg2+2\pi}{3}-(\psi_2\psi'_{1x}-\psi_1\psi'_{2x})\cos\tfrac{\arg2+2\pi}{3}\right),\\
\nu'_{ay} = {} & \tfrac{1}{3}|\kappa_1|^{-5/3}\left((\phi_1\phi'_{1y}+\phi_2\phi'_{2y})\cos\tfrac{\arg1+2\pi}{3}+(\phi_2\phi'_{1y}-\phi_1\phi'_{2y})\sin\tfrac{\arg1+2\pi}{3}\right)\\
& +\tfrac{1}{3}|\kappa_2|^{-5/3}\left((\psi_1\psi'_{1y}+\psi_2\psi'_{2y})\cos\tfrac{\arg2+2\pi}{3}+(\psi_2\psi'_{1y}-\psi_1\psi'_{2y})\sin\tfrac{\arg2+2\pi}{3}\right),\\
\nu'_{by} = {} & \tfrac{1}{3}|\kappa_1|^{-5/3}\left((\phi_1\phi'_{1y}+\phi_2\phi'_{2y})\sin\tfrac{\arg1+2\pi}{3}-(\phi_2\phi'_{1y}-\phi_1\phi'_{2y})\cos\tfrac{\arg1+2\pi}{3}\right)\\
& +\tfrac{1}{3}|\kappa_2|^{-5/3}\left((\psi_1\psi'_{1y}+\psi_2\psi'_{2y})\sin\tfrac{\arg2+2\pi}{3}-(\psi_2\psi'_{1y}-\psi_1\psi'_{2y})\cos\tfrac{\arg2+2\pi}{3}\right)
\end{aligned}
\tag{63}
$$

$$
\begin{aligned}
\phi_1\phi'_{1x}+\phi_2\phi'_{2x} = {} & \tfrac{\tilde{x}}{4}+\tfrac{|\Delta|+r^2-\chi^2}{8\sqrt{|\Delta|}}\left(\sin\tfrac{\theta}{2}-\tfrac{\tilde{x}}{\tilde{y}}\cos\tfrac{\theta}{2}\right)-\tfrac{r^2-\chi^2}{8\tilde{y}}\sin\theta\\
\psi_1\psi'_{1x}+\psi_2\psi'_{2x} = {} & \tfrac{\tilde{x}}{4}-\tfrac{|\Delta|+r^2-\chi^2}{8\sqrt{|\Delta|}}\left(\sin\tfrac{\theta}{2}-\tfrac{\tilde{x}}{\tilde{y}}\cos\tfrac{\theta}{2}\right)-\tfrac{r^2-\chi^2}{8\tilde{y}}\sin\theta\\
\phi_1\phi'_{1y}+\phi_2\phi'_{2y} = {} & \tfrac{\tilde{y}}{4}+\tfrac{|\Delta|+r^2+\chi^2}{8\sqrt{|\Delta|}}\left(\tfrac{\tilde{y}}{\tilde{x}}\sin\tfrac{\theta}{2}-\cos\tfrac{\theta}{2}\right)-\tfrac{r^2+\chi^2}{8\tilde{x}}\sin\theta\\
\psi_1\psi'_{1y}+\psi_2\psi'_{2y} = {} & \tfrac{\tilde{y}}{4}-\tfrac{|\Delta|+r^2+\chi^2}{8\sqrt{|\Delta|}}\left(\tfrac{\tilde{y}}{\tilde{x}}\sin\tfrac{\theta}{2}-\cos\tfrac{\theta}{2}\right)-\tfrac{r^2+\chi^2}{8\tilde{x}}\sin\theta
\end{aligned}
\tag{64}
$$

$$
\begin{aligned}
\phi_2\phi'_{1x}-\phi_1\phi'_{2x}= &\ \frac{\tilde{y}}{4}+\frac{\sqrt{|\Delta|}}{8}\left(\frac{\tilde{x}}{\tilde{y}}\sin\frac{\theta}{2}-3\cos\frac{\theta}{2}\right)-\frac{r^2-\chi^2}{8\sqrt{|\Delta|}}\left(\frac{\tilde{x}}{\tilde{y}}\sin\frac{\theta}{2}+\cos\frac{\theta}{2}\right)\\
&-\frac{\tilde{x}}{8}\left(\tan\frac{\theta}{2}+\cot\frac{\theta}{2}\right)+\frac{(r^2-\chi^2)\tilde{x}}{8|\Delta|}\left(\tan\frac{\theta}{2}-\cot\frac{\theta}{2}\right)\\
\psi_2\psi'_{1x}-\psi_1\psi'_{2x}= &\ \frac{\tilde{y}}{4}-\frac{\sqrt{|\Delta|}}{8}\left(\frac{\tilde{x}}{\tilde{y}}\sin\frac{\theta}{2}-3\cos\frac{\theta}{2}\right)+\frac{r^2-\chi^2}{8\sqrt{|\Delta|}}\left(\frac{\tilde{x}}{\tilde{y}}\sin\frac{\theta}{2}+\cos\frac{\theta}{2}\right)\\
&-\frac{\tilde{x}}{8}\left(\tan\frac{\theta}{2}+\cot\frac{\theta}{2}\right)+\frac{(r^2-\chi^2)\tilde{x}}{8|\Delta|}\left(\tan\frac{\theta}{2}-\cot\frac{\theta}{2}\right)\\
\phi_2\phi'_{1y}-\phi_1\phi'_{2y}= &\ -\frac{\tilde{x}}{4}-\frac{\sqrt{|\Delta|}}{8}\left(3\sin\frac{\theta}{2}-\frac{\tilde{y}}{\tilde{x}}\cos\frac{\theta}{2}\right)-\frac{r^2+\chi^2}{8\sqrt{|\Delta|}}\left(\sin\frac{\theta}{2}+\frac{\tilde{y}}{\tilde{x}}\cos\frac{\theta}{2}\right)\\
&+\frac{\tilde{y}}{8}\left(\tan\frac{\theta}{2}+\cot\frac{\theta}{2}\right)+\frac{(r^2+\chi^2)\tilde{y}}{8|\Delta|}\left(\tan\frac{\theta}{2}-\cot\frac{\theta}{2}\right)\\
\psi_2\psi'_{1y}-\psi_1\psi'_{2y}= &\ -\frac{\tilde{x}}{4}+\frac{\sqrt{|\Delta|}}{8}\left(3\sin\frac{\theta}{2}-\frac{\tilde{y}}{\tilde{x}}\cos\frac{\theta}{2}\right)+\frac{r^2+\chi^2}{8\sqrt{|\Delta|}}\left(\sin\frac{\theta}{2}+\frac{\tilde{y}}{\tilde{x}}\cos\frac{\theta}{2}\right)\\
&+\frac{\tilde{y}}{8}\left(\tan\frac{\theta}{2}+\cot\frac{\theta}{2}\right)+\frac{(r^2+\chi^2)\tilde{y}}{8|\Delta|}\left(\tan\frac{\theta}{2}-\cot\frac{\theta}{2}\right)
\end{aligned}
\tag{65}
$$

Figure Caption

Figure 1
A longer-wavelength image of edge-on spiral galaxy NGC 4565 (Courtesy of Jarrett *et al* [1]). The central bulge is easily recognized. The disk density is the product of that in perpendicular direction and that in horizontal direction (see (50)).

Figure 2
Left panel is the simulated galaxy NGC 3275. The right panel is the real galaxy image at H-band wavelength (Courtesy of Eskridge *et al* [12])

Figure 3
Left panel is the simulated galaxy NGC 3275. The right panel is the noise, arms, central bulge resulted from the subtraction of the left panel from the real galaxy image at H-band wavelength (Courtesy of Eskridge *et al* [12])

Figure 4
Left panel is the simulated galaxy NGC 4930. The right panel is the noise, arms, central bulge resulted from the subtraction of the left panel from the real galaxy image at H-band wavelength (Courtesy of Eskridge *et al* [12])

Figure 5
Left panel is the simulated galaxy NGC 5701. The right panel is the noise, arms, central bulge resulted from the subtraction of the left panel from the real galaxy image at H-band wavelength (Courtesy of Eskridge *et al* [12])

Figure 6
Left panel is the simulated galaxy NGC 6782. The right panel is the noise, arms, central bulge resulted from the subtraction of the left panel from the real galaxy image at H-band wavelength (Courtesy of Eskridge *et al* [12])

Figure 7
Left panel is the examples of the simulated galaxy arms for NGC 3275. The right panel is the corresponding Darwin curves of "ellipse" shape. The corresponding orthogonal curves of "hyperbola" shape are not displayed. Our concept of rational structure is based on the orthogonal Darwin curves.

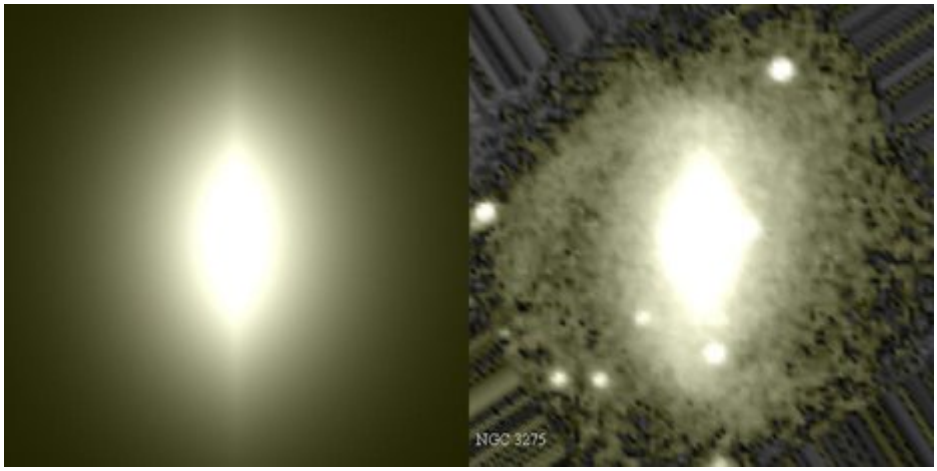

Figure 2: Left panel is the simulated galaxy NGC 3275. The right panel is the real galaxy image at H-band wavelength (Courtesy of Eskridge *et al* [12])

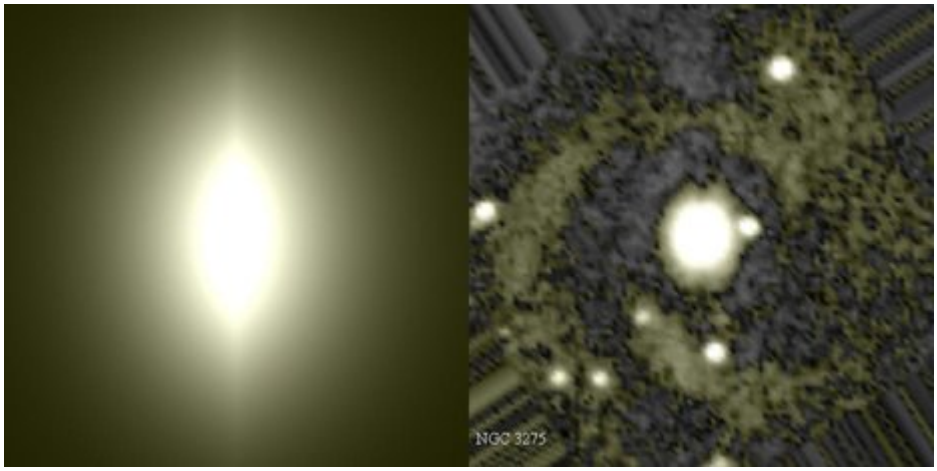

Figure 3: Left panel is the simulated galaxy NGC 3275. The right panel is the noise, arms, central bulge resulted from the subtraction of the left panel from the real galaxy image at H-band wavelength (Courtesy of Eskridge *et al* [12])

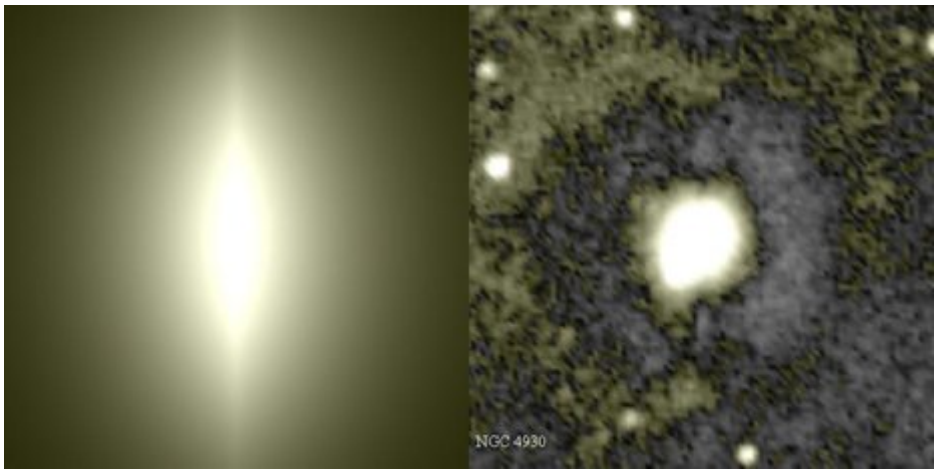

Figure 4: Left panel is the simulated galaxy NGC 4930. The right panel is the noise, arms, central bulge resulted from the subtraction of the left panel from the real galaxy image at H-band wavelength (Courtesy of Eskridge *et al* [12])

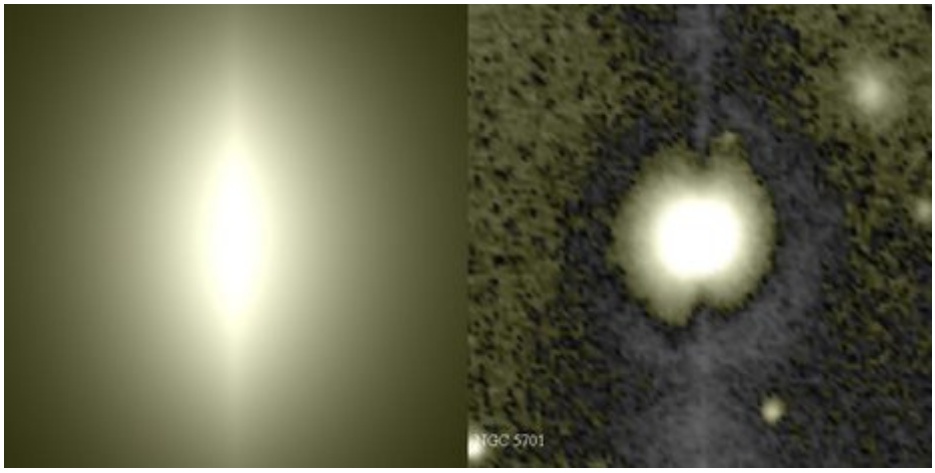

Figure 5: Left panel is the simulated galaxy NGC 5701. The right panel is the noise, arms, central bulge resulted from the subtraction of the left panel from the real galaxy image at H-band wavelength (Courtesy of Eskridge *et al* [12])

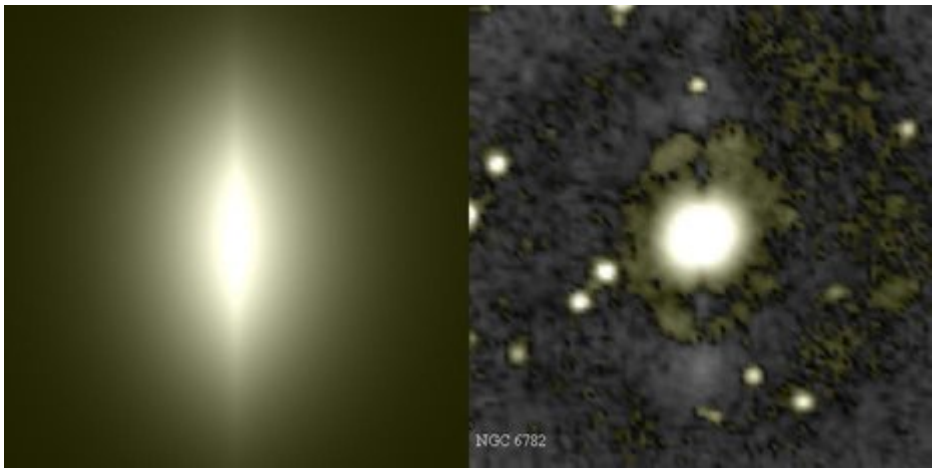

Figure 6: Left panel is the simulated galaxy NGC 6782. The right panel is the noise, arms, central bulge resulted from the subtraction of the left panel from the real galaxy image at H-band wavelength (Courtesy of Eskridge *et al* [12])

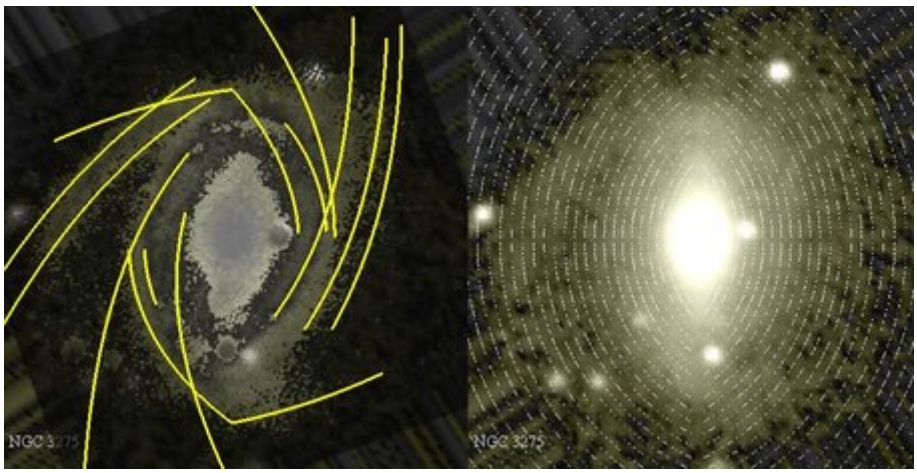

Figure 7: Left panel is the examples of the simulated galaxy arms for NGC 3275. The right panel is the corresponding Darwin curves of "ellipse" shape. The corresponding orthogonal curves of "hyperbola" shape are not displayed. Our concept of rational structure is based on the orthogonal Darwin curves.